ORIGINAL RESEARCH

Conventional ultrasound combined with contrast-enhanced ultrasound quantitative analysis for diagnosing lung cancer metastases in neck lymph nodes

Anran Wang[1], Mei Zhang[1], Shufang Xiang[1], Can Liu[1],*

[1]Department of Ultrasonography, The First Affiliated Hospital of Yangtze University, 434000 Jinzhou, Hubei, China

*Correspondence
lc_liucan888@163.com
(Can Liu)

Abstract

Lung cancer remains one of the most common malignant tumors. Identifying cervical lymph node metastases is important to stage lung cancer, evaluate patients' prognosis and select appropriate treatments. This study evaluated the utility of conventional ultrasound combined with contrast-enhanced ultrasound (CEUS) quantitative analysis in diagnosing lung cancer metastases in the lymph nodes of the neck. The cervical lymph nodes of 39 patients with primary lung cancer who underwent CEUS and ultrasound-guided needle biopsy were assessed. Routine type B ultrasound was used to record the morphology of the lymph nodes and the presence of lymphatic hilum structure. The Vuebox quantitative analysis software was used to collect lymph node CEUS peak enhancements (PE), rise time (RT) and fall time (FT). The receiver operating characteristic (ROC) curve was used to evaluate the diagnostic value of various parameters and imaging characteristics. The cohort comprised 26 cervical lymph nodes with lung cancer metastasis and 13 cervical lymph nodes with reactive hyperplasia. Most hilum of lymph gland were absent in the metastasis group (92.30%), most lymph nodes showed a full shape (80.77%), and few were irregularly shaped (19.23%). Most hilum of lymph gland were present in the hyperplasia group (76.95%) and showed a full shape (61.54%). The PE of the metastasis group (4852.29 a.u) was significantly lower than the hyperplasia group (11,464.70 a.u), while the difference between RT and FT indicators was not significant. ROC analysis showed that combined PE of the quantitative ultrasound contrast analysis and the presence of the lymphatic phylum structure showed satisfactory diagnostic ability for detecting lung cancer lymph node metastasis in the neck (sensitivity 73.10%, specificity 76.90%, accuracy 48.73%, $p = 0.004$). Conventional ultrasound observation of lymph node structure combined with quantitative analysis of peak enhancement of contrast-enhanced ultrasound showed promising value for diagnosing lung cancer metastatic lymph nodes.

Keywords

Ultrasonography; CEUS; Quantitative analysis; Cervical lymph node; Metastatic lymph nodes

1. Introduction

Lung cancer remains one of the most common malignant tumors worldwide. It is ranked first in cancer incidence and mortality in men and is also at the forefront in cancer incidence and mortality in women [1, 2]. However, due to its deep location and indolent course, some young patients might have already developed lymph node metastasis by the time of diagnosis [3]. The first symptom of lung cancer is supraclavicular lymph node metastasis due to cervical lymph node drainage. Thus, identifying cervical lymph node metastases, especially in supraclavicular lymph nodes, is important to accurately stage lung cancer, evaluate patients' prognosis and select appropriate treatments [4].

There are many methods for detecting cervical metastatic lymph nodes in clinics, including palpation, 2D ultrasound, Color Doppler Flow Imaging (CDFI), trans intravenous contrast ultrasound imaging, Computer Tomography (CT), Magnetic Resonance Imaging (MRI), *etc*. Among all imaging techniques, conventional ultrasound is more convenient as it can show the morphological characteristics obtained that are not easily obtained by CT and MRI, but it is still difficult to accurately distinguish benign and malignant lymph nodes [5]. Conventional ultrasound can be used to observe the size, shape, boundary, and hilar structure of lymph nodes. Color Doppler flow imaging can be used to preliminarily observe the blood flow signals inside and around lymph nodes. As a new qualitative ultrasound diagnostic technique, contrast-enhanced

ultrasound has been widely used in clinical practice. There are relatively mature research results in the qualitative analysis of abdominal organs, superficial organs, lymph nodes, and so on. For the differential diagnosis of benign and malignant cervical lymph nodes, certain reference information can be provided for clinical differential diagnosis by observing the contrast agent perfusion method of the target lymph node, whether the perfusion is uniform, compared with surrounding tissues, the relative intensity of the target lymph node perfusion, the speed of perfusion and clearance, and whether there is a perfusion defect area [6]. The trans-intravenous injection of ultrasound contrast agent microbubbles is commonly used in clinics. This contrast agent enters systemic circulation through the pulmonary capillaries to reach the lesion *via* systemic blood flow and produces a large amount of backscattering in the ultrasonic acoustic field to enhance the contrast between blood flow within microvessels and tissue and observe tissue microcirculation perfusion in real time. Contrast-enhanced ultrasound (CEUS) is more sensitive than color Doppler flow imaging for detecting low-speed microvascular blood flow [7]. The quantitative analysis of ultrasound contrast uses software to analyze and process the region of interest (ROI) during ultrasound contrast to form the time-intensity curve (TIC), obtain specific contrast quantitative imaging parameters and provide a valuable objective reference for clinical differential diagnosis.

2. Methods

2.1 Patient data

Patients with primary lung cancer and abnormal cervical lymph nodes treated at Jingzhou First People's Hospital from January 2021 to May 2022 were included if they met the following criteria (Table 1). All patients provided and signed informed consent before receiving intravenous ultrasound angiography and ultrasound-guided crude needle biopsy. A total of 39 patients were included in the study. The patient characteristics are list in the table below (Table 2).

2.2 Conventional ultrasound examination

An 8–13 MHz, high-frequency line array probe was obtained using a Type LOGIQ E9 Color Doppler Ultrasound Diagnostics instrument (GE, Boston, MA, USA). The patient was asked to overextend their neck and fully expose the site to be examined. The maximum display section of the lymph node in the best position was selected [8] to observe and record their morphology, including the hilum of lymph gland and portal blood flow signal.

2.3 Contrast-enhanced ultrasound examination

Using the contrast mode of the above instrument, a contrast agent consisting of the SonoVue ultrasonic contrast agent (F200905Z, Bracco, Mediolanium, Lombardia, Italy), 59 mg of sulfur hexafluoride gas and 25 mg of white lyophilized powder was used and administered with 5 mL of 0.9% sodium chloride solution into a bottle, which was shaken repeatedly

for 15 seconds to prepare a microbubble suspension. Then, 2.5 mL of the contrast microbubble suspension was quickly injected through the intravenous channel, followed by 5 mL normal saline flushing to keep the probe stable, and the contrast process was recorded.

2.4 Quantitative analysis of contrast ultrasound

Digital Imaging and Communications in Medicine (DICOM) data were exported using the Vuebox CEUS quantitative analysis software (Bracco Suisse SA-Software Applications, 31 route de la Galaise, CH-1228 Plan-les-Ouates, Switzerland). The software preset automatically optimized the ultrasound instrument model and superficial high-frequency probe, and lymph nodes were delineated as ROI. An attempt was made to have the ROI area cover the boundary of the target lymph node and compensate for motions. A TIC was prepared, and the analysis report was exported before selecting the peak enhancements (PE), rise time (RT) and fall time (FT) for statistical analysis (Fig. 1).

2.5 Histopathological examination

All patients underwent ultrasound-guided crude needle puncture histological biopsy for pathological analysis. The cases were divided into a cervical lymph node metastasis group or benign reactive hyperplasia of cervical lymph node group according to the pathological diagnosis and the inclusion and exclusion criteria.

2.6 Statistical method

The Excel 2013 software (Microsoft, Redmond, WA, USA) was used to record the data, and the SPSS v25.0 software (IBM, Armonk, NY, USA) was used for statistical analysis. Quantitative data that met the normal distribution are represented by mean $\pm$ standard deviation ($\bar{x} \pm s$). The means were compared between the groups using two independent sample t-tests. Data that did not fit a normal distribution are shown as median (interquartile spacing), and comparisons between such groups were performed using the Wilcoxon rank sum test. Qualitative data are expressed using frequencies and percentages, and rates were compared using the Chi-square test. ROC was used to evaluate the sensitivity, specificity, accuracy and area under the curve (AUC) of the qualitative CEUS parameters. The Youden index was applied to determine the optimal cutoff value. Differences were considered statistically significant for p-values < 0.05.

3. Results

3.1 Pathological results

An ultrasound-guided crude needle puncture histological biopsy was performed for final pathological analysis, which identified 26 cases of lung cancer cervical lymph node metastasis (Fig. 2) and 13 cases of benign reactive hyperplasia of cervical lymph nodes (Fig. 3, Table 2). And divided into metastatic group and benign group according to pathological results.

T A B L E 1. Inclusion and exclusion criteria.

Inclusion criteria:

● Abnormal lymph node morphology findings such as enlargement, full shape, uneven internal echo, unclear hilum of lymph gland and no obvious portal blood flow signal on routine ultrasonography.

● Underwent trans-intravenous injection ultrasound angiography.

● Obtained more accurate pathological results upon ultrasound-guided downward needle biopsy.

● Pathology showing either lung cancer cervical lymph node metastasis or benign reactive hyperplasia.

Exclusion criteria:

● Poor contrast ultrasound video quality images due to patient's movement or excessive respiratory movement.

● Incomplete contrast data due to short ultrasound imaging data.

● Inaccurate diagnosis due to a low amount of biopsy materials or unsatisfactory sampling.

T A B L E 2. Patient characteristics.

Case	Age/Sex	Lymphatic hilum	Form	PE (a.u)	RT (s)	FT (s)	Histopathological results
1	74/M	unclear	full	4492.84	5.09	8.90	Metastatic pulmonary squamous cell carcinoma in right cervical lymph node
2	65/M	unclear	irregular	4208.52	4.64	9.20	Metastatic pulmonary squamous cell carcinoma with necrosis in left cervical lymph node
3	50/M	unclear	full	2625.43	4.23	8.12	Metastatic pulmonary adenocarcinoma in right cervical lymph node
4	44/F	unclear	full	982.19	8.68	21.91	Metastatic pulmonary adenocarcinoma with necrosis in left cervical lymph node
5	69/M	unclear	full	7890.22	4.50	8.23	Metastatic pulmonary adenocarcinoma in left cervical lymph node
6	62/M	unclear	full	2313.58	6.16	18.45	Metastatic pulmonary adenocarcinoma in left cervical lymph node
7	67/M	unclear	full	1527.55	3.74	5.74	Metastatic pulmonary adenocarcinoma in bilateral cervical lymph nodes
8	50/M	unclear	irregular	5334.33	4.41	8.17	Metastatic pulmonary adenocarcinoma in right cervical lymph node
9	69/F	unclear	full	374.93	7.70	15.75	Metastatic pulmonary adenocarcinoma in left cervical lymph node
10	67/F	unclear	full	3644.33	5.16	9.17	Metastatic pulmonary adenocarcinoma in right cervical lymph node
11	62/M	unclear	full	3348.67	6.52	11.34	Metastatic pulmonary adenocarcinoma in left cervical lymph node
12	57/M	unclear	full	11,132.36	4.41	8.16	Metastatic pulmonary adenocarcinoma in right cervical lymph node
13	64/F	clear	full	6672.36	3.66	6.51	Metastatic pulmonary adenocarcinoma in right cervical lymph node
14	71/M	unclear	irregular	9196.25	4.39	7.69	Metastatic pulmonary adenocarcinoma in right cervical lymph node
15	62/F	unclear	full	7332.32	6.16	13.21	Metastatic pulmonary adenocarcinoma in left cervical lymph node
16	81/M	unclear	full	3769.91	7.89	15.09	Metastatic pulmonary adenocarcinoma in right cervical lymph node
17	33/M	clear	full	4400.17	3.39	6.20	Metastatic pulmonary adenocarcinoma in right cervical lymph node
18	50/F	unclear	full	5211.73	4.76	8.64	Metastatic pulmonary adenocarcinoma in left cervical lymph node

TABLE 2. Continued.

Case	Age/Sex	Lymphatic hilum	Form	PE (a.u)	RT (s)	FT (s)	Histopathological results
19	75/M	unclear	full	287.08	7.44	14.17	Metastatic pulmonary small cell carcinoma in left cervical lymph node
20	76/M	unclear	full	6266.74	3.89	6.60	Metastatic pulmonary small cell carcinoma in left cervical lymph node
21	63/M	unclear	full	986.71	6.41	16.97	Metastatic pulmonary small cell carcinoma in right cervical lymph node
22	71/M	unclear	full	11,819.44	7.17	13.67	Metastatic pulmonary small cell carcinoma in right cervical lymph node
23	51/F	unclear	full	7681.00	5.65	10.76	Metastatic pulmonary small cell carcinoma in left cervical lymph node
24	69/F	unclear	irregular	48,029.41	4.46	8.49	Metastatic pulmonary small cell carcinoma in left cervical lymph node
25	69/M	unclear	irregular	35,322.00	7.75	15.27	Metastatic pulmonary small cell carcinoma in right cervical lymph node
26	71/M	unclear	full	7402.96	4.44	9.04	Metastatic pulmonary small cell carcinoma in left cervical lymph node
27	44/F	clear	full	21,477.25	3.62	6.64	Benign reactive hyperplasia of left cervical lymph node
28	29/F	clear	normal	18,879.30	5.11	8.95	Benign reactive hyperplasia of left cervical lymph node
29	71/M	clear	full	25,632.73	4.54	8.56	Benign reactive hyperplasia of left cervical lymph node
30	66/F	clear	normal	20,678.66	4.27	7.79	Benign reactive hyperplasia of left cervical lymph node
31	66/M	clear	full	13,206.89	9.32	28.39	Benign reactive hyperplasia of right cervical lymph node
32	57/F	unclear	full	6564.69	5.15	9.90	Benign reactive hyperplasia of left cervical lymph node
33	59/M	clear	full	11,464.70	4.02	7.11	Benign reactive hyperplasia of left cervical lymph node
34	34/M	clear	normal	5532.02	4.04	7.08	Benign reactive hyperplasia of left cervical lymph node
35	75/M	unclear	full	31,391.12	3.09	4.85	Benign reactive hyperplasia of left cervical lymph node
36	62/M	clear	full	1134.16	4.79	8.46	Benign reactive hyperplasia of left cervical lymph node
37	14/F	clear	full	5409.28	4.38	7.89	Benign reactive hyperplasia of right cervical lymph node
38	38/F	clear	normal	3042.5	6.30	13.36	Benign reactive hyperplasia of right cervical lymph node
39	49/F	unclear	normal	5718.56	5.58	8.80	Benign reactive hyperplasia of left cervical lymph node

PE: peak enhancements; RT: rise time; FT: fall time.
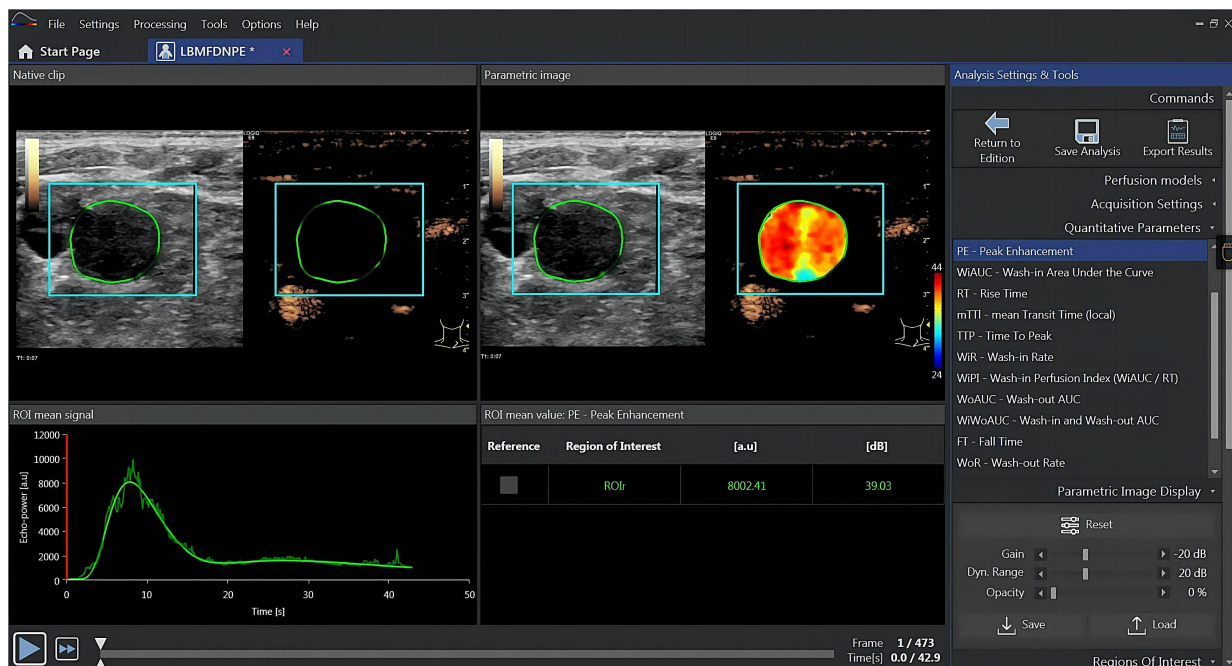
F I G U R E 1. Vuebox analysis interface for metastatic lymph nodes in the neck of lung cancer.
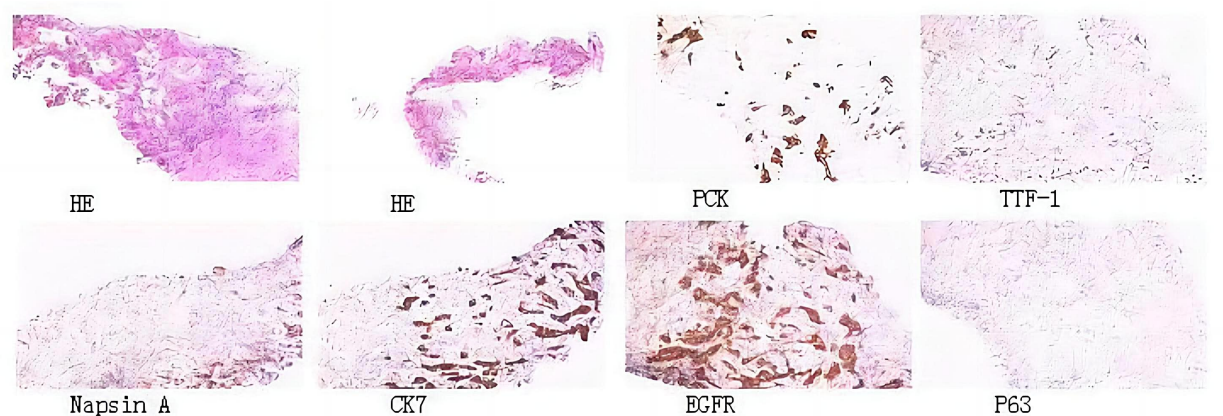

F I G U R E 2. Pathological image of cervical lymph node metastasis of lung cancer. HE: haematoxylin and eosin; PCK: pan cytokeratin; TTF-1: thyroid transcription factor-l; CK7: cytokeratin 7; EGFR: epidermal growth factor receptor; P63: recombinant tumor protein P63.
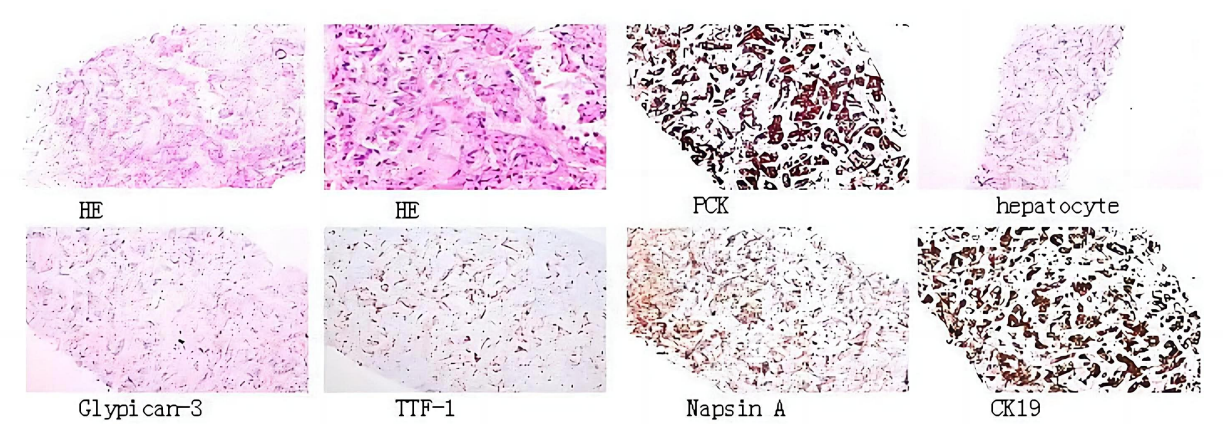

F I G U R E 3. Pathological image of cervical benign reactive hyperplasia lymph nodes. HE: haematoxylin and eosin; PCK: pan cytokeratin; TTF-1: thyroid transcription factor-l; CK19: cytokeratin 19.

3.2 Conventional ultrasound results

Of the 26 cervical lymph nodes with lung cancer metastasis, 22 had a full morphology, while 4 were irregularly shaped. 8 of the 13 cases of benign reactive hyperplasia of the cervical lymph nodes showed morphological fullness (Fig. 4), while the remaining 5 showed a normal morphology. The three morphologies (full, normal, irregular) significantly differed between the two groups ($p < 0.001$) (Table 3).

Moreover, the lymphatic hilum structure was indistinct in 24 of the 26 cervical lymph nodes containing lung cancer metastasis. The blood flow was mixed or peripheral type (Fig. 5), and only two cases of hilum of lymph gland exhibited portal-type blood flow. Only three of the 13 cases with benign reactive hyperplasia of the cervical lymph nodes showed unclear hilar structures, presenting with nonhilar blood flow. Comparatively, the remaining 10 cases showed visible hilar blood flow signals. The rate of unclear lymphatic hilum significantly differed between the two groups ($p < 0.001$), which was found to be higher in the metastasis group than in the benign group (92.30% *vs.* 23.08%) (Table 3).

3.3 Quantitative analysis of contrast ultrasound results

The PE significantly differed between the benign reactive hyperplasia group and the lung cancer metastasis group ($p = 0.037$). Specifically, the PE was significantly lower in the metastasis group than in the benign group (4852.29 a.u *vs.* 11,464.70 a.u), while RT and FT did not significantly differ between the two groups ($p > 0.05$) (Table 3).

3.4 Diagnostic efficacy of quantitative parameters

PE cutoff value ≤ 1330.855 units showed good diagnostic results for diagnosing malignant lymph nodes ($p = 0.037$), while the diagnostic effectiveness of RT and FT were low ($p > 0.05$). Quantitative CEUS analysis showed that the PE sensitivity, specificity, accuracy and AUC were 84.60%, 7.70%, 91.66% and 0.293, respectively. PE combined with the presence or absence of lymphatic hilus at a cutoff value of 0.902 units showed good diagnostic ability for detecting metastatic lymph nodes ($p = 0.004$). The sensitivity, specificity, accuracy and AUC of the CEUS quantitative analysis for PE combined with the presence or absence of lymphatic hilus were 73.10%, 76.90%, 48.73% and 0.790, respectively (Fig. 6 and Table 4).

4. Discussion

Given the rapid economic development and increase in population aging in an increasing number of countries and regions, controlling the incidence of lung cancer remains challenging as its risks and incidence are known to increase with age. Developments in medical technology have helped the early diagnosis of lung cancer. Specifically, assessing the status of cervical lymph node metastasis is an important step for accurately staging lung cancer because metastasis in this region is closely related to the prognosis of lung cancer and the choice of treatments.

Solely relying on the size of cervical lymph nodes may not accurately differentiate between benign and malignant lymph nodes as they usually depend on the partition of the neck and the patient's age [9]. Moreover, metastatic lymph nodes usually appear fuller and tend to be round, whereas lymph nodes with benign reactive hyperplasia are usually larger but flatter and rounder [10]. The presence or absence of hilum of lymph gland can also be used as identification criteria for benign and malignant cervical lymph nodes [11]. Although the above differential diagnostic characteristics of two-dimensional ultrasound are not absolute, they have considerable diagnostic value. Using multicenter imaging omics, some scholars developed an ultrasonic imaging omics model based on cervical lymph nodes using two-dimensional ultrasound images to improve the differential diagnostic efficiency of cervical lymph node tuberculosis, cervical lymphoma, cervical lymph node reactive hyperplasia and metastatic lymph nodes [12]. Benign reactive lymph nodes have a normal lymph node morphology and vascular anatomy with a normal hilar structure, while metastatic lymph nodes have neovascularization that penetrates the capsule. Conventional color Doppler ultrasound can analyze the flow and perfusion pattern of lymph nodes, and the injection of an ultrasound contrast agent can significantly improve the sensitivity and specificity of malignant lymph node neovascularization [13]. It is reported that its resolution may even surpass that of CT and MRI [14], indicating ultrasound imaging to be of great value for the follow-up of malignant tumors after radiotherapy and chemotherapy and to evaluate the presence of recurrence or lymph node metastases [15].

The qualitative diagnosis obtained visually by observing the ultrasound contrast process might be too subjective. TIC obtained by processing and analyzing DICOM data with quantitative analysis software, such as Vuebox, can provide an objective basis. At present, quantitative analyses in clinics using PE and AUC can reflect the contrast concentration of contrast perfusion, while RT, arrival time (AMT) and FT can reflect the efficiency of contrast perfusion and regression to provide valuable differential diagnosis information for different types of pathological lesions [16].

Ying *et al.* [10] used arrival time parametric imaging technology to analyze the arrival time of contrast agents around the lymph nodes, which can provide more information for the differential diagnosis of superficial lymph nodes [17]. Nie *et al.* [18] quantitatively analyzed the TIC, PE, RT and AUC for three parameters and combined this information with observations of lymph node ultrasound images in contrast perfusion mode and enhancement mode to improve the differential diagnostic accuracy of head and neck lymph node status [18].

This study collected the conventional two-dimensional ultrasound imaging features of the cervical lymph nodes of lung cancer patients mainly including the enlargement of lymph node morphology and the absence of lymph node hilum. The corresponding node ultrasound contrast DICOM data were used to generate TIC with time as the abscissa and the contrast perfusion intensity as the ordinate. This curve extracted accurate quantitative data, including PE, RT and FT. RT and FT can objectively reflect the node contrast perfusion and regression rates such as fast forward and fast backward, slow forward and
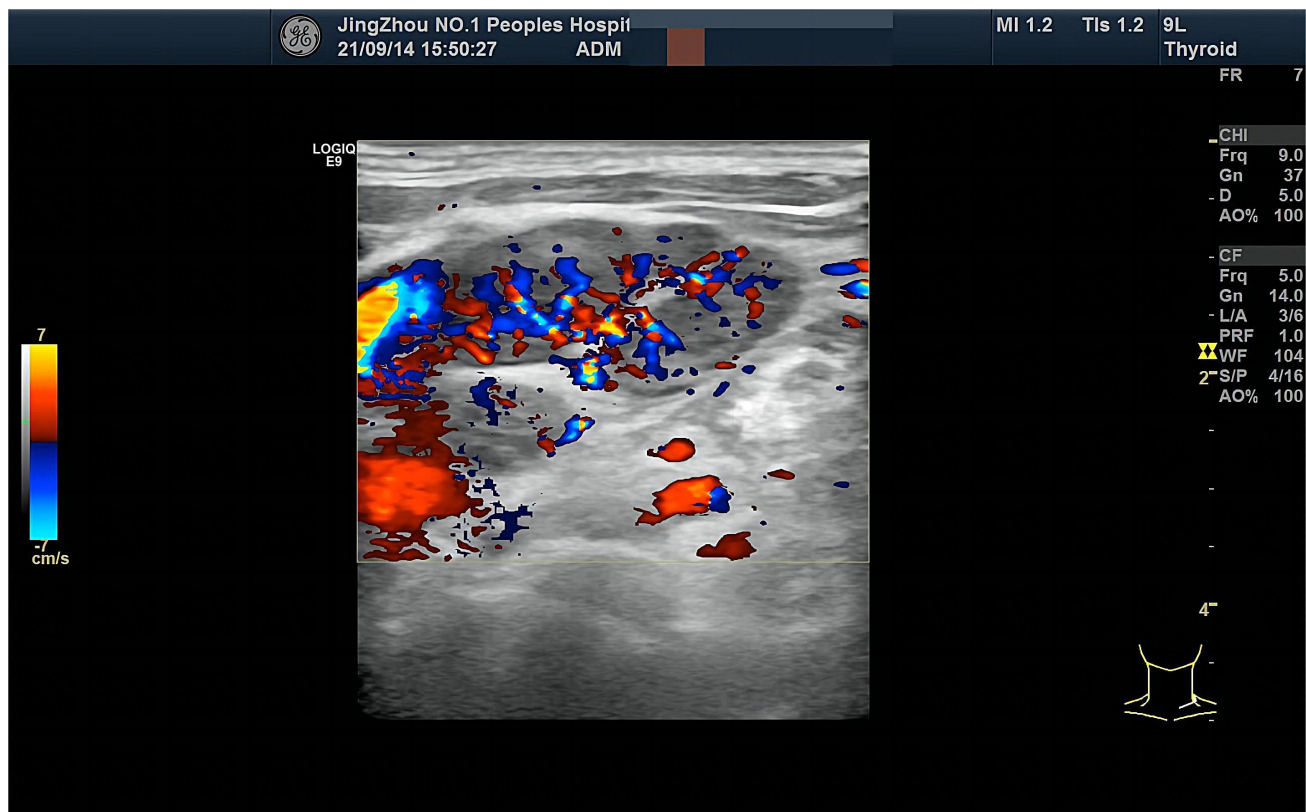
F I G U R E 4. Benign reactive hyperplastic lymph nodes. FR: frame rat; CHI: contrast harmonic imaging; Frq: frequency; Gn: Gain; D: depth; AO: acoustic output; PRF: pulse repetition frequency; L/A: line density/frame average; WF: wall filter; S/P: spatial filter/ packet size; CF: color flow.
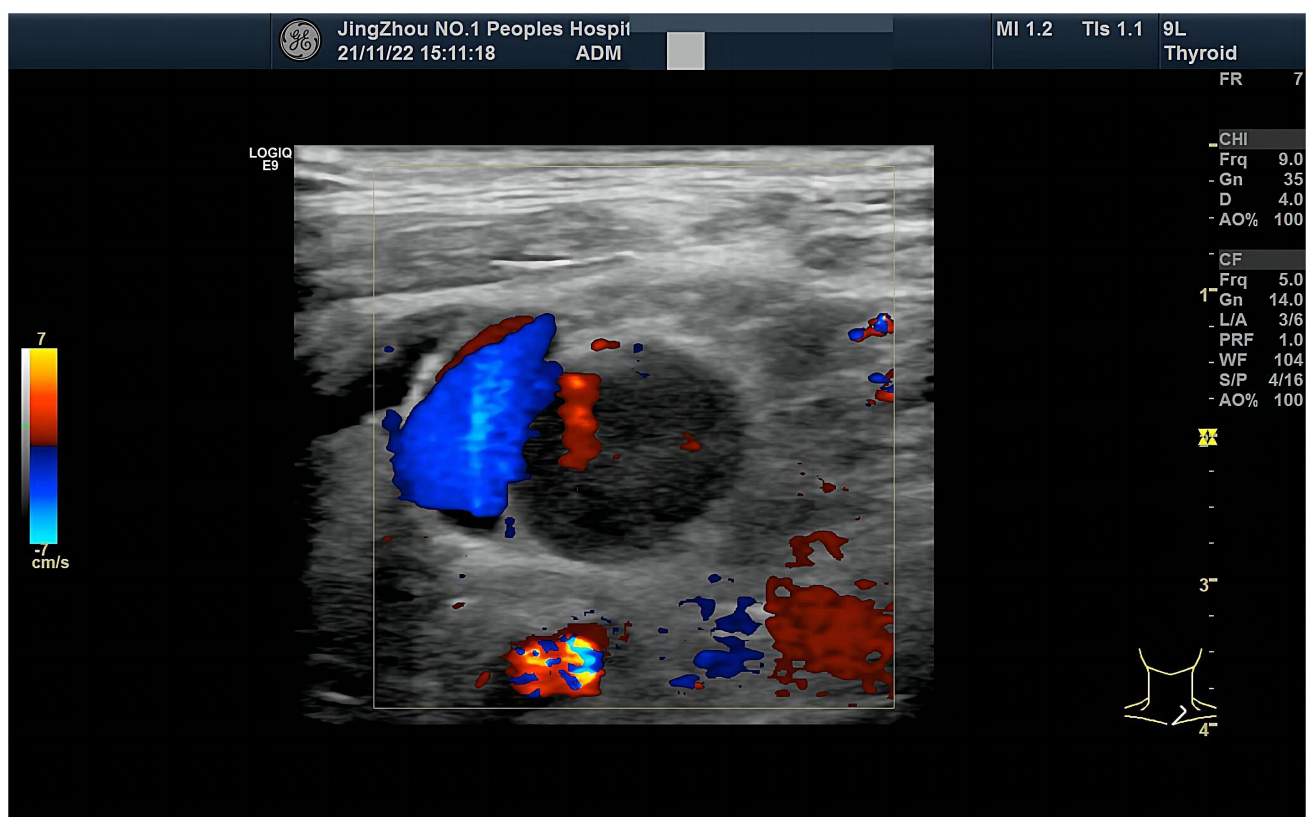

F I G U R E 5. Metastatic lymph nodes of lung cancer. FR: frame rat; CHI: contrast harmonic imaging; Frq: frequency; Gn: Gain; D: depth; AO: acoustic output; PRF: pulse repetition frequency; L/A: line density/frame average; WF: wall filter; S/P: spatial filter/packet size; CF: color flow.

TABLE 3. Wilcoxon rank sum test for difference analysis.

Index	Metastatic lymph nodes of lung cancer (n = 26)	Benign reactive hyperplastic lymph nodes (n = 13)	$Z/_{c^2}$	p
PE				
Median (Min, Max)	4852.29 (2547.47, 7733.31)	11,464.70 (5470.65, 21,077.96)	4.349	0.037
RT				
Median (Min, Max)	4.93 (4.41, 6.68)	4.54 (4.03, 5.365)	1.350	0.245
FT				
Median (Min, Max)	9.11 (8.15, 14.40)	8.46 (7.095, 9.425)	1.878	0.171
Lymphatic hilum				
unclear	24 (92.30%)	3 (23.08%)	19.500	<0.001
clear	2 (7.70%)	10 (76.92%)		
Form				
full	21 (80.77%)	8 (61.54%)		
normal	0 (0.00%)	5 (38.46%)	15.486	<0.001
irregular	5 (19.23%)	0 (0.00%)		

Note: PE was significantly lower in the metastasis group than in the benign group (4852.29 vs. 11,464.70). The rate of unclear lymphatic hilum was higher in the metastasis group than in the benign group (92.30% vs. 23.08%). PE: peak enhancements; RT: rise time; FT: fall time.
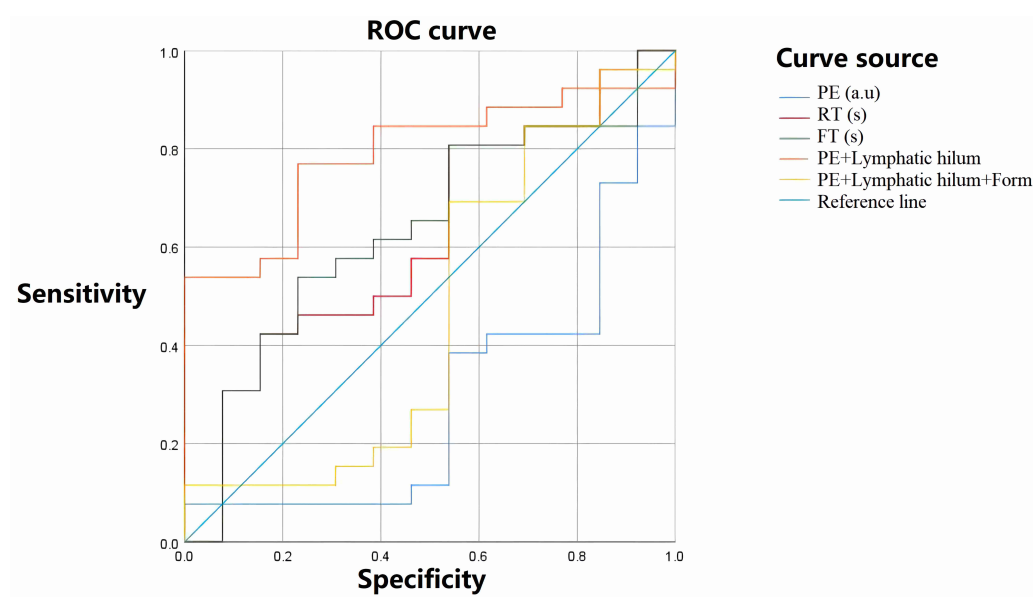

FIGURE 6. ROC curve figure. PE: peak enhancements; RT: rise time; FT: fall time; ROC: receiver operating characteristic.

TABLE 4. ROC curve table.

Index	Cutoff	Sensitivity	Specificity	Accuracy	AUC (95% CI)	p
PE	1330.855	0.846	0.077	0.9166	0.293 (0.116, 0.470)	0.037
RT	4.385	0.808	0.462	0.6362	0.615 (0.425, 0.805)	0.245
FT	8.995	0.538	0.769	0.4116	0.636 (0.450, 0.822)	0.171
PE + lymphatic hilum	0.902	0.731	0.769	0.4873	0.790 (0.648, 0.931)	0.004
PE + lymphatic hilum + form	0.941	0.692	0.462	0.5997	0.467 (0.254, 0.681)	0.743

Note: the area under the ROC curve was greater than 0.5, suggesting that the diagnostic test had certain diagnostic significance. PE cutoff value ≤1330.855 units showed good diagnostic accuracy for diagnosing malignant lymph nodes (p = 0.037). PE combined with the presence or absence of lymphatic hilus at a cutoff value of 0.902 units showed good diagnostic accuracy for detecting metastatic lymph nodes (p = 0.004). ROC: receiver operating characteristic; AUC: area under the curve; CI: Confidence Interval; PE: peak enhancements; RT: rise time; FT: fall time.

slow backward, fast forward and slow backward, *etc*. Sonja Schwarz *et al.* [19] used contrast ultrasound TIC analysis of the liver to show that the RT in the TIC time index could help distinguish between benign and malignant liver lesions. Further, Lu Qing *et al.* [20] found that differences in the degrees of differentiation of liver cells and metastatic liver cancer differed in the contrast ultrasound TIC of multiple time indices.

Cervical metastatic lymph nodes of lung cancer show neovascularization of the lymph node capsule, which changes the microcirculation perfusion in the lymph nodes similar to contrast enhanced ultrasound differences between liver space occupying lesions and normal liver tissues, maybe in the time index of TIC, appeared some differences from reactive proliferative lymph nodes. Thus, the RT and FT time index were selected in this study, but our final results did not show any significant difference in these two between the two groups of lymph nodes. A possible explanation for the difference in PE between the two groups could be that enlarged lymph nodes due to lung cancer metastases may exhibit partial necrosis, partial contrast, low contrast or even a lack of contrast perfusion. Consequently, when the software analyzed the contrast agent, the overall perfusion peak intensity was shown as low and benign reactive hyperplastic lymph nodes may not show necrosis. Software analysis of the ROI of the contrast agent showed that the overall perfusion PE value was higher in the hyperplasia group than in the metastasis group [21]. Further, the ROC analysis also indicated that PE had good diagnostic effects (sensitivity 84.6%, accuracy 91.66%, $p = 0.037$), while its specificity remained very low (7.70%). The absence of the lymphatic hilus is one of the most common malignant criteria for conventional type B ultrasound [11]. Color Doppler blood flow imaging and ultrasound contrast imaging can be more accurate and intuitive methods to diagnose lymphatic gate structures and the presence of portal-type blood flow. In this present study, the morphology of cervical lymph nodes was recorded by visual observation. However, the specific division of cervical lymph nodes and patients' age varied. In addition, some of the enlarged reactive hyperactive lymph nodes also exhibited relatively full image characteristics, making the image features more subjective compared with other collected parameters and imaging features. Based on the ROC assessment, combining the peak intensity of CEUS quantitative analysis with the presence or absence of the lymphatic gate structure demonstrated a good diagnostic effect for detecting metastatic lymph nodes in the neck of lung cancer patients (sensitivity 73.10%, specificity 76.90%, accuracy 48.73%, $p = 0.004$). Although adding the characteristics of lymph node morphology slightly increased the diagnostic accuracy (59.97%), the specificity remained low (46.20%).

Due to the regional and time limit of this study, the number of samples collected was small, leading to insufficient cervical metastatic lymph node cases with different pathological types, such as lung adenocarcinoma, squamous cell carcinoma and small cell lung cancer, for statistical analysis and comparison between groups and might have affected the final statistical results. In addition, this study did not have any limitations on the size of target lymph nodes. During the actual inspection process, it was challenging to use conventional ultrasound to identify the presence of lymphatic hilum in smaller lymph nodes, which might be resolved by increasing the sample size and using multicenter settings to analyze conventional ultrasound images *via* artificial intelligence imageomics technology to avoid the impact of human subjective factors.

5. Conclusions

In conclusion, conventional ultrasound observations of lymph node structures combined with quantitative analysis of the peak intensity of contrast-enhanced ultrasound have important values in diagnosing metastatic lymph nodes in lung cancer. Specifically, this strategy can help evaluate the stage, prognosis and choice of treatment options for lung cancer. However, this study remained subject to considerable limitations due to the number of samples, regional limitations and human factors, urging the need for further research to confirm these findings.

AVAILABILITY OF DATA AND MATERIALS

All data generated or analyzed during this study are included in this published article.

AUTHOR CONTRIBUTIONS

ARW and CL—Conception and design; CL—Administrative support; MZ and SFX—Provision of study materials or patients; ARW—Collection and assembly of data, Data analysis and interpretation; All authors —Manuscript writing and Final approval of manuscript.

ETHICS APPROVAL AND CONSENT TO PARTICIPATE

The study was conducted in accordance with the Declaration of Helsinki (as revised in 2013). The study was approved by the Ethics Committee of Jingzhou First People's Hospital (NO.: KY202226), and individual consent for this retrospective analysis was waived.

CONFLICT OF INTEREST

The authors declare no conflict of interest.

REFERENCES

[1] Liu ZC, Li ZX, Zhang Y, Zhou T, Zhang JY, You WC, *et al.* Interpretation on the report of Global Cancer Statistics 2020. Journal of Multidisciplinary Cancer Management. 2021; 7: 1–14. (In Chinese)

[2] Khaltaev N, Axelrod S. Global lung cancer mortality trends and lifestyle modifications: preliminary analysis. Chinese Medical Journal. 2020; 133: 1526–1532.

[3] Ma TT, Wan YX, Shi L. Pathological characteristics and prognosis of patients with primary lung cancer. The Practical Journal of Cancer. 2019; 34: 1835–1838. (In Chinese)

[4] Xie X, Li X, Tang W, Xie P, Tan X. Primary tumor location in lung cancer: the evaluation and administration. Chinese Medical Journal. 2022; 135: 127–136.

[5] Chammas MC, Macedo TAA, Lo VW, Gomes AC, Juliano A, Cerri GG. Predicting malignant neck lymphadenopathy using color duplex sonography based on multivariate analysis. Journal of Clinical Ultrasound. 2016; 44: 587–594.

[6] Mei M, Ye L, Quan J, Huang P. Contrast-enhanced ultrasound for the differential diagnosis between benign and metastatic superficial lymph nodes: a meta-analysis. Cancer management and research. 2018; 10: 4987–4997.

[7] Liu HF, Xiao JD. Flow imaging of residual neck lymph nodes in nasopharyngeal carcinoma by contras-enhanced ultrasonography after radiotherapy. Journal of Central South University (Medical sciences). 2010; 35: 861–863. (In Chinese)

[8] Wang DL, Yang GY, Shao YQ, Zhang WZ. Contrast-enhanced ultrasound for research on tuberculosis of axillary lymph node. Journal of Medical Research. 2013; 42: 187–189.

[9] Giacomini CP, Jeffrey RB, Shin LK. Ultrasonographic evaluation of malignant and normal cervical lymph nodes. Seminars in Ultrasound, CT and MRI. 2013; 34: 236–247.

[10] Ying M, Bhatia KS, Lee YP, Yuen HY, Ahuja AT. Review of ultrasonography of malignant neck nodes: greyscale, Doppler, contrast enhancement and elastography. Cancer Imaging. 2014; 13: 658–669.

[11] Bialek EJ, Jakubowski W, Szczepanik AB, Maryniak RK, Prochorec-Sobieszek M, Bilski R, et al. Vascular patterns in superficial lymphomatous lymph nodes: a detailed sonographic analysis. Journal of Ultrasound. 2007; 10: 128–134.

[12] Liu Y, Chen J, Zhang C, Li Q, Zhou H, Zeng Y, et al. Ultrasound-based radiomics can classify the etiology of cervical lymphadenopathy: a multi-center retrospective study. Frontiers in Oncology. 2022; 12: 856605.

[13] Sidhu PS, Cantisani V, Dietrich CF, Gilja OH, Saftoiu A, Bartels E, et al. The EFSUMB guidelines and recommendations for the clinical practice of contrast-enhanced ultrasound (CEUS) in non-hepatic applications: update 2017 (long version). Ultraschall in der Medizin. 2018; 39: e2–e44.

[14] Dudau C, Hameed S, Gibson D, Muthu S, Sandison A, Eckersley RJ, et al. Can contrast-enhanced ultrasound distinguish malignant from reactive lymph nodes in patients with head and neck cancers? Ultrasound in Medicine & Biology. 2014; 40: 747–754.

[15] Weskott HP. Contrast-enhanced ultrasound in the diagnostic workup of lymph nodes. Radiologe. 2018; 58: 563–571. (In German)

[16] Xin L, Yan Z, Zhang X, Zang Y, Ding Z, Xue H, et al. Parameters for contrast-enhanced ultrasound (CEUS) of enlarged superficial lymph nodes for the evaluation of therapeutic response in lymphoma: a preliminary study. Medical Science Monitor. 2017; 23: 5430–5438.

[17] Yin S, Cui Q, Fan Z, Yang W, Yan K. Diagnostic value of arrival time parametric imaging using contrast-enhanced ultrasonography in superficial enlarged lymph nodes. Journal of Ultrasound in Medicine. 2019; 38: 1287–1298.

[18] Nie J, Ling W, Yang Q, Jin H, Ou X, Ma X. The value of CEUS in distinguishing cancerous lymph nodes from the primary lymphoma of the head and neck. Frontiers in Oncology. 2020; 10: 473.

[19] Schwarz S, Clevert DA, Ingrisch M, Geyer T, Schwarze V, Rübenthaler J, et al. Quantitative analysis of the time-intensity curve of contrast-enhanced ultrasound of the liver: differentiation of benign and malignant liver lesions. Diagnostics. 2021; 11: 1244.

[20] Lu Q, Zhang X, Han H, Huang B, Ding H, Wang W. Value of perfusion parameters for differentiating hepatocellular carcinoma and liver metastasis with hypervascularity and a normal hepatic background on contrast-enhanced ultrasound imaging. Journal of Ultrasound in Medicine. 2019; 38: 2601–2608.

[21] Lerchbaumer MH, Wakonig KM, Arens P, Dommerich S, Fischer T. Quantitative multiparametric ultrasound (mpUS) in the assessment of inconclusive cervical lymph nodes. Cancers. 2022; 14: 1597.